24th COBEM - 2017

24th ABCM International Congress of Mechanical Engineering
December 3-8, 2017, Curitiba, PR, Brazil

COBEM-2017-1988
CONTROL SYSTEMS FOR FLUTTER SUPPRESSION OF A TYPICAL SECTION

Gefferson Cleuber Silva
Flávio José Silvestre
Maurício Vicente Donadon
Osmar Souza Santos
Antônio B. G. Neto
Roberto Gil A. Silva
Tiago S. S. Versiani
Rafael Mendes Bertolin
Department of Aeronautics, Instituto Tecnológico de Aeronáutica, São José dos Campos, Brazil
geffersonports@hotmail.com, flaviojs@ita.br, donadon@ita.br, osmar@ita.br, antoniobgn@gmail.com, gil@ita.br, versiani.t@gmail.com, rafaelmbufsj@gmail.com

Abstract. *Flutter is the most important phenomenon in aeroelastics. Important concerns associated to it are the difficulties to predict flutter and to control it. This paper describes the use of a typical airfoil section that presents a simple binary flutter behavior as a testbed for the development of active and passive control systems for flutter instability suppression. The wing section is a NACA 0012 airfoil with a trailing edge control surface used as actuator. The active control strategy consists of a stability augmentation system with output feedback to maintain the system stable in closed-loop. The equations of motion were developed using Lagrange's equations and the Principle of Virtual Work. The aerodynamic loads are estimated by an unsteady time-domain formulation based on Wagner's function. The passive control system employs a shape memory alloy to induce an additional torsional stiffness related to its crystallographic phase transformation. Experimental results show considerable reduction of the oscillation amplitudes at a relative low cost for both active and passive strategies, and that the use of shape memory alloys for aeroelastic control is promising.*

Keywords: *aeroelasticity, flutter suppression, shape memory alloy, typical section, linear quadractic regulator*

1. INTRODUCTION

The flutter phenomenon can be considered as one of the most discussed and studied aeroelastic problem in the open literature. It is an unstable self-excited vibration in which the structure extracts energy from the air stream and often results in catastrophic structural failure. Classical binary flutter occurs when the aerodynamic forces associated with motion in two modes of vibration cause the modes to couple in an unfavourable manner, Wright and Cooper (2008).

The study and understanding of this aeroelastic instability is very important for its prediction, since the critical flutter speed sometimes define the flight envelope of the aircraft. When it is not feasible to avoid this instability through structural or aerodynamical changes, a possible and widely reported form to increase the aircraft flight envelope is the development of control systems for flutter suppression.

The development of control systems for flutter suppression is related to the need of changing the dynamic behavior of aeroelastic systems by applying control forces to suppress the instability and maintain the system stable, Vipperman *et al.* (1998). Since then, various control techniques for different approaches of flutter occurrence have been studied and developed in the last decades, as can be seen in recent works Hwang and Pi (1984) and (Dykman *et al.*, 2013).

Currently, a major challenge for the aeronautical industry is the development of structures capable of continuously adapting to different flight conditions, constituting the so-called adaptive or smart structures. Adaptive structures are able to adapt to different operating conditions in response to external disturbances or control inputs, Janocha *et al.* (1999).

In the last four decades, one of the most interesting and studied smart material as an option for adaptive structures applications are the Shape Memory Alloys (SMA) due to their unique property, the shape memory effect (SME). The SME is associated to deformation of the SMA at low temperature phase (martensite) and its recovery to the original shape by the reverse transformation of the crystallographic phase upon heating to a critical temperature.The vibration control using SMA is based primarily on changing the system stiffness, as can be seen in Donadon and de Faria (2016) and Silva *et al.* (2017).

This work describes the use of a typical wing section with degrees of freedom of pitch (around y axis) and plunge

(in z axis direction) as an aeroelastic apparatus for study and development of active and passive control systems for acceleration reduction when the unstable behavior of the wing is reached. The active control system is based on the feedback of estimated pitch rate, with gain scheduling via the linear-quadratic regulator (LQR) theory. The passive control system applies a shape memory wire introduced in the torsional axis to increase torsional stiffness as a function of the temperature.

The wing section is a NACA 0012 airfoil with 80 cm of wingspan, 29 cm of chord and has an articulated flap controlled by a servomotor. The wing is mounted on a movable base that emulates the degrees of freedom of pitch and plunge. The movable base is supported by a fixed one, as can bee seen in Fig. 1.

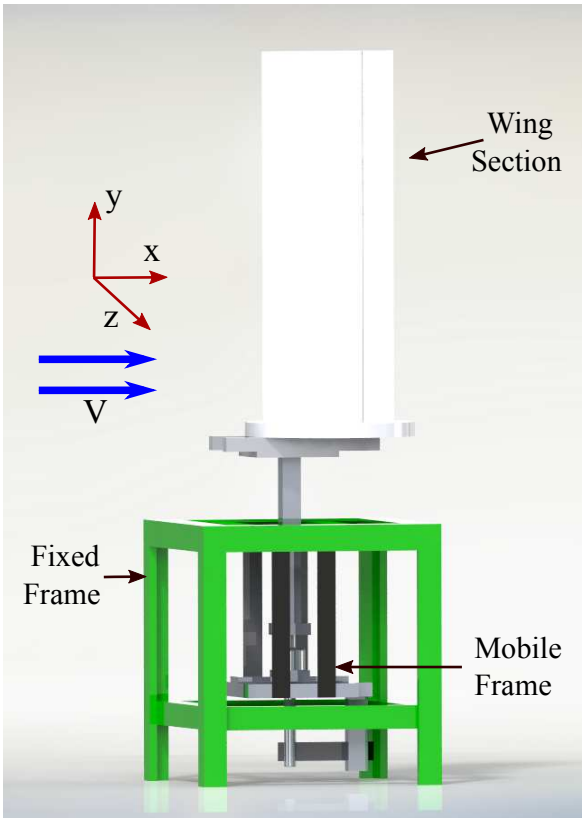

Figure 1. Illustration of the aeroelastic apparatus.

The wing section used in this work presents an experimental critical flutter speed at 14 m/s. To verify the pitch and plunge frequencies coupling with the increase of the airspeed, the Fast Fourier Transform (FFT) of the accelerometer signal located at the leading edge of the wing was performed for some velocities of interest about the critical one. The Figure 2 shows the FFT response for each velocity normalized by the maximum value.

2. EQUATIONS OF MOTION

Using h and θ as generalized coordinates, Lagrange's equation can be applied to derive the equations of motion of the system. The principle of virtual work is used to obtain the expressions of the generalized forces. Rewritten in matrix form we have:

$$\begin{bmatrix} m & S_\theta \\ S_\theta & I_\theta \end{bmatrix} \begin{Bmatrix} \ddot{h} \\ \ddot{\theta} \end{Bmatrix} + \begin{bmatrix} c_h & 0 \\ 0 & c_\theta \end{bmatrix} \begin{Bmatrix} \dot{h} \\ \dot{\theta} \end{Bmatrix} + \begin{bmatrix} K_h & 0 \\ 0 & K_\theta \end{bmatrix} \begin{Bmatrix} h \\ \theta \end{Bmatrix} + \begin{bmatrix} S_\beta \\ I_\beta + b\,(e-a)\,S_\beta \end{bmatrix} \ddot{\beta}_c = \begin{Bmatrix} -L \\ M_{ea} \end{Bmatrix} \tag{1}$$

where b is the semi-chord; m and I_θ are the mass and the moment of inertia relative to the elastic axis (EA) of the movable part of the system, which is chordwise at a distance be from the centroid; S_θ is its the static mass moment relative to EA; I_β and S_β are the flap's moment of inertia and static mass moment relative to the articulation axis, which is chordwise at a position ba relative to the centroid; c_h and c_θ are the structural damping coefficients in pitch and plunge; and K_h and K_θ are the pitch and plunge stiffnesses respectively; L and M_{ea} and lift and pitch moment around EA.

Potential flow theory of a thin airfoil was used to calculate the aerodynamic lift and pitch moment. An unsteady formulation based on Wagner's indicial function in the time domain has been applied, considering Jones' exponential

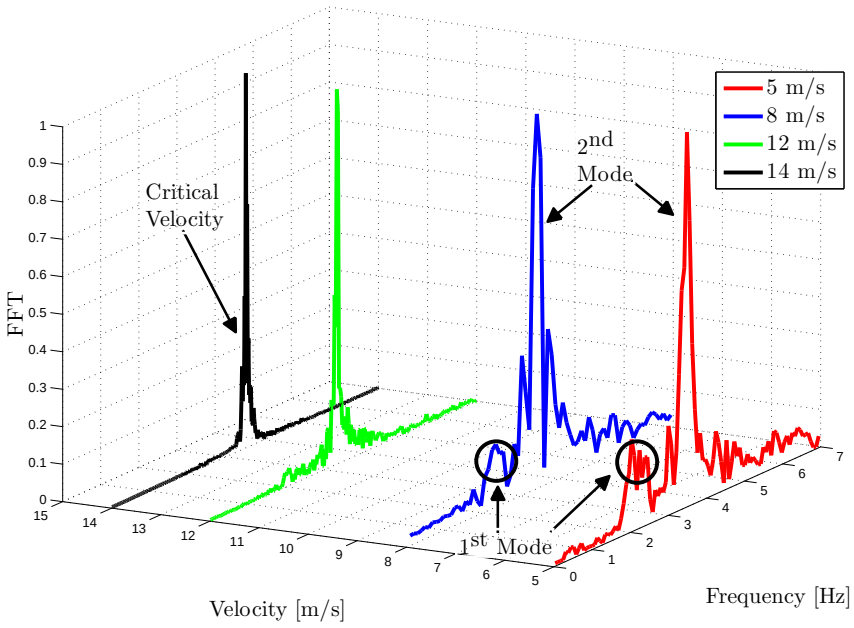

Figure 2. FFT response evolution for different air speeds.

approximation, as in (Silvestre and Luckner, 2015), resulting in the following expressions:

$$\begin{aligned} L = & - \rho b^2 V \dot{\beta} \left(e\sqrt{1-e^2} - \cos^{-1} e \right) \\ & - \rho b^3 \ddot{\beta} \left(e \cos^{-1} e - \frac{1}{3} \left(2+e^2\right) \sqrt{1-e^2} \right) \\ & + \pi b^2 \rho \left(\ddot{h} + V\dot{\theta} - ba\ddot{\theta} \right) \\ & + 2\pi\rho V b \left(Q_{3/4} + \lambda_1 + \lambda_2 \right), \end{aligned} \tag{2}$$

$$\begin{aligned} M_{ea} = & - \pi\rho b^2 V Q_{3/4} + b\left(a+\frac{1}{2}\right)\left(2\pi\rho V b \left[Q_{3/4}+\lambda_1+\lambda_2\right]\right) \\ & - \rho b^2 V^2 \beta \left(e\sqrt{1-e^2} - \cos^{-1} e \right) \\ & - \rho b^3 V \dot{\beta} \left\{ \frac{1}{3}\sqrt{1-e^2}\left(e^2-1\right) - (e-a)\left[e\sqrt{1-e^2} - \cos^{-1} e \right] \right\} \\ & - \rho b^4 \ddot{\beta} \left\{ \left(\frac{1}{8}+e^2\right)\cos^{-1} e - \frac{1}{8} e \sqrt{1-e^2}\left(7+2e^2\right) \right. \\ & + \left. (e-a)\left[\frac{1}{3}\sqrt{1-e^2}\left(2+e^2\right) - e\cos^{-1} e \right] \right\} \\ & + \pi b^2 \rho \left[V\dot{h} + ba\ddot{h} + V^2\theta - b^2\left(\frac{1}{8}+a^2\right)\ddot{\theta} \right], \end{aligned} \tag{3}$$

where λ_1 and λ_2 represent the aerodynamic lag to respond to a change in the downwash in 3/4 chord position, $Q_{3/4}$, and can be determined through the following first order differential equations:

$$\dot{\lambda}_1(t) = -0.041\left(\frac{V}{b}\right)\lambda_1(t) - 0.165\dot{Q}_{3/4}(t), \tag{4}$$

$$\dot{\lambda}_2(t) = -0.32\left(\frac{V}{b}\right)\lambda_2(t) - 0.335\dot{Q}_{3/4}(t). \tag{5}$$

and $\dot{Q}_{3/4}$ is the acceleration of the downwash in the position of 3/4 chord.

Grouping Equations from 2 to 5 leads to the following model in state-space form:

$$\dot{x} = \mathbf{A}x + \mathbf{B}\beta_c + \mathbf{B_p}\dot{\beta}_c + \mathbf{B_{pp}}\ddot{\beta}_c, \tag{6}$$

where the state vector x is given by,

$$x = \left\{ \begin{array}{c} h \\ \theta \\ \dot{h} \\ \dot{\theta} \\ \lambda_1 \\ \lambda_2 \end{array} \right\}. \tag{7}$$

3. ACTIVE CONTROL SYSTEM

This work has the purpose of design an active control system for acceleration reduction of the system when its unstable behavior related to the flutter phenomenon is achieved, still maintaining the system stable in closed-loop. For this, a stability augmentation system (SAS) is developed. The pitch rate is estimated ($\tilde{\dot{\theta}}$) by measured accelerations at the leading and the trailing edges (Ac_{LE} and Ac_{TE}, respectively), and used as a feedback signal.

The resulting control signal is converted to a flap deflection by a servomechanism. The deflection deflection in turn generates additional damping, thus reducing the oscillations.

The feedback gain $\mathbf{K}$ is calculated minimizing the following quadractic performance index

$$J = \frac{1}{2}\int_0^\infty (x^T\mathbf{Q}x + u^T\mathbf{R}u)dt \tag{8}$$

which penalises disturbances in the state variables x and the required control u. The minimization of J leads to the solution of the following Lyapunov equation

$$\mathbf{A_c}^T\mathbf{P} + \mathbf{P}\mathbf{A_c} + \mathbf{C}^T\mathbf{K}^T\mathbf{R}\mathbf{K}\mathbf{C} + \mathbf{Q} = 0 \tag{9}$$

where $\mathbf{A_c} \equiv (\mathbf{A} - \mathbf{B}\mathbf{K}\mathbf{C})$.

The servomotor used as the actuator is limited in amplitude depending on actuation frequency and hinge moment due to aerodynamic loads. The limit flap deflection of $\pm 10^\circ$ about the experimental critical flutter speed was achieved through a set of experimental tests. This actuator limitation is considered into the choice process of the weight matrix Q.

Weighting matrices $\mathbf{Q}$ and $\mathbf{R}$ have been selected to attain performance with required control, so that

$$\mathbf{Q} = [I]_{6\times 6} \tag{10}$$

$$\mathbf{R} = \left[\begin{array}{c} 50 \end{array} \right] \tag{11}$$

resulting in $\mathbf{K} = -0.1202^\circ/(^\circ/s)$. The data set for the aeroelastic apparatus is shown in Table 1.

The simulated acceleration at the trailing edge of the typical section with air speed of 15 m/s due to an impulse input applied at t = 1 s is shown in Figure 3. The system is in open loop in the beginning, and the SAS is turned on at $t = 6$ s, reducing the amplitude of oscillation.

The required control signal is compared to the effective control signal applied to the system considering the limitations of the actuator, Figure 4, t, where except for an initial peak of 13.5° in the flap deflection, all control signals remain achievable from the standpoint of the limitations of the actuation system.

V-g diagrams of the system in both open-loop and closed-loop configurations are shown in Figure 5. This diagram has been obtained by analyzing the eigenvalues of the state matrix of the system. The closed-loop system has an increased flutter speed of 16.65 m/s, i.e., there is an increase of about 15.3 % in the critical flutter speed.

To experimentally validate the designed SAS, wind tunnel tests were accomplished with the aeroelastic apparatus, in both open and closed-loop. The wing section was instrumented with 3 accelerometers located on the leading edge, trailing edge, and base of the apparatus.

The acceleration measurements taken at the trailing edge and leading edge are received on one of the A/D channels of a DSpace acquisition system for estimating the pitch rate. The estimated pitch rate is then fed back into the SAS and the resulting control signal is sent to the servo actuation which translates it into flap deflections opposing the oscillations in order to provide an increase in the system damping.

Experimental test was performed at 15 m/s using a feedback gain of $\mathbf{K} = -0.180$. This difference between the experimentally tuned and numerically calculated gains is due to differences between the experimental and numerical

Table 1. Numerical data for simulations.

Property	**Value**	**Unit**
Semi-chord (b)	0.145	m
Mass (m)	13.5	kg
Plunge frequency (f_h)	2.38	Hz
Pitch frequency (f_θ)	4.29	Hz
Location of hinge line, in semi-chords	0.6	–
Control surface chord (c_{cs})	0.06	m
Plunge damping ratio (ζ_h)	0.03	–
Pitch damping ratio (ζ_θ)	0.03	–
Air density (ρ)	1.119	kg/m^3
Location of elastic axis, in semi-chords (a)	-0.1379	–
c.g. coordinate from e.a. (x_θ), in semi-chords	0.0275	–
Radius of gyration of the airfoil referred to a (r_θ)	0.064	m

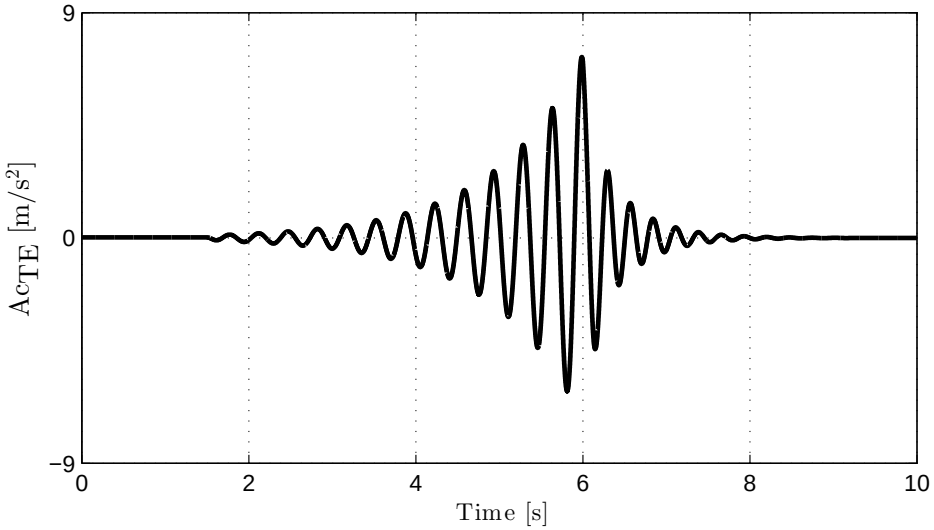

Figure 3. Simulated acceleration at the trailing edge with control loop closed at $t = 6$ s and velocity of 15 m/s.

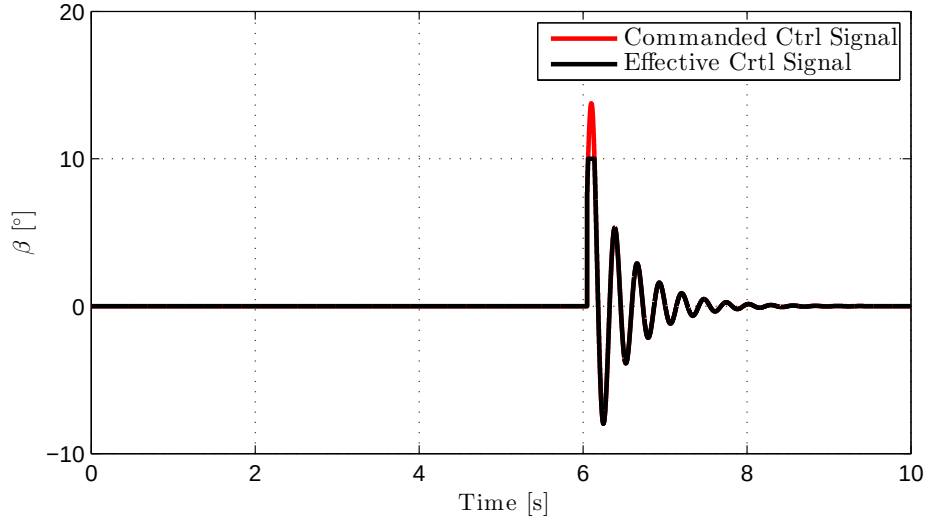

Figure 4. Simulated control surface deflection at $t = 6$ s and velocity of 15 m/s.

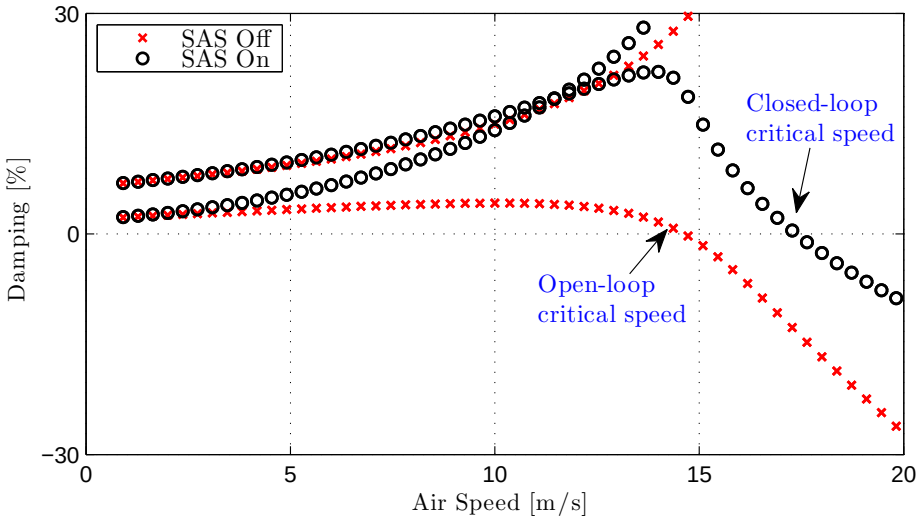

Figure 5. V-g diagram for the open and closed-loop systems.

models of the system regarding not-modeled phenomena and non-linearities such as the vortices produced at the exit of the wind tunnel.

Figure 6 shows the leading edge acceleration at 15 m/s (top), and the commanded and measured control signals (bottom). The test begins in open loop and at some point the SAS is turned on.

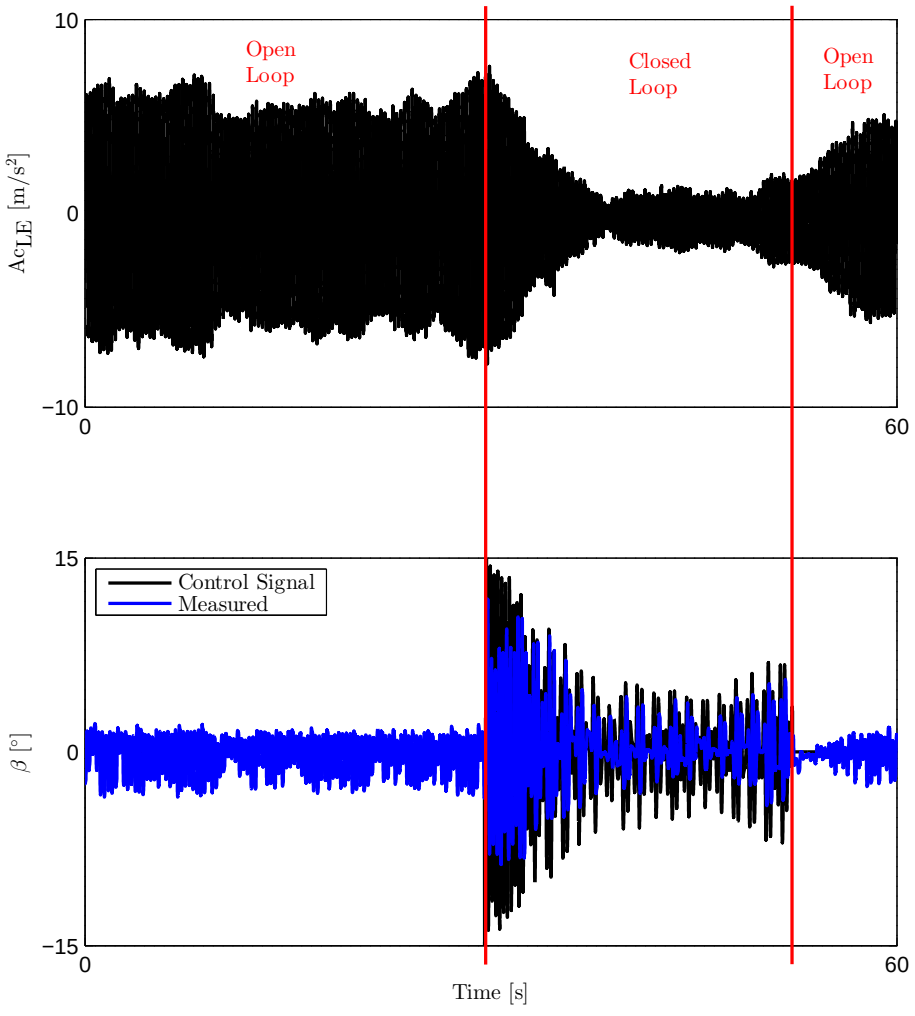

Figure 6. Experimental response with closed-loop control with velocity of 15 m/s.

Using the same feedback gain applied in the previous case for the SAS and incrising the wind tunnel speed, the control system is not capable to reduce the oscillations due to the actuator limitions in front of a larger aerodynamic loads. Figure 7 shows the closed-loop system response at the speed of 16.5 m/s, where the flap deflections are not sufficient for suppression the oscillatory behavior of the wing.

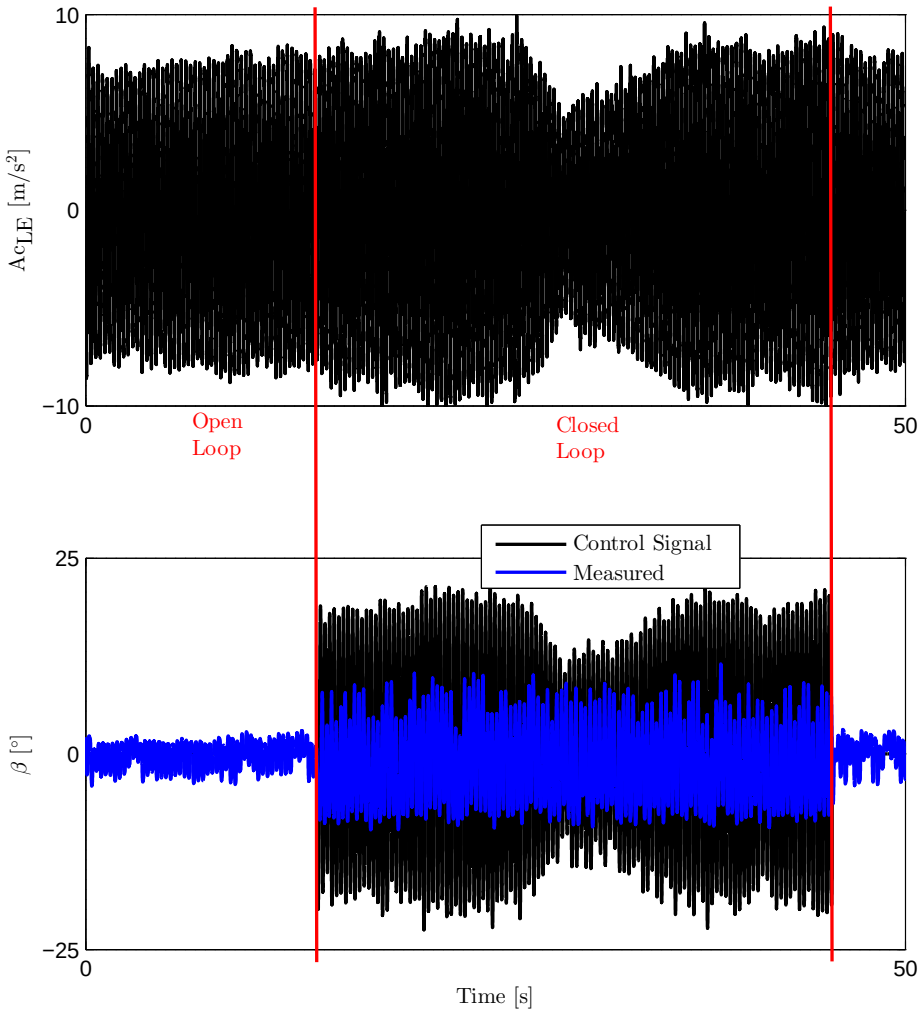

Figure 7. Experimental response with closed-loop control with velocity of 16.5 m/s.

In general, the experimental results are fairly satisfactory, reducing considerably the oscillations for the velocities analyzed, despite the many limitations of the system, and the non-modeled phenomena. The experimental critical velocity was increased approximately 8%, presenting performance very similar to 10% obtained in work developed by De Marqui Jr *et al.* (2004), with the average vibration reduction of -12.3958 dB. Note that although the oscillations are attenuated with the SAS on, oscillations of small amplitude still appear as a result of disturbances produced by the wind tunnel, and limitations of servo performance.

4. PASSIVE CONTROL SYSTEM

The passive aeroelastic control technique proposed in this paper is based on the application of a SMA wire to increase the torsional stiffness by the crystallographic phase transformation of the NiTi wire in the typical section.

The wire is connected to the torsional axis of the aeroelastic apparatus as shown in Figure 8. In the torsion mode, the wire is tensioned, providing additional torsional stiffness to the wing. If the wire temperature increases, the phase transformation of the SMA leads to an increase in the tension necessary to deform the wire, increasing the additional torsion stiffness provided to the wing.

As shown in the Figure 8, the provided wire stiffness is a function of system parameters, such as: torsion shaft radius R_t, wire length L, and axial load F delivered by the wire as a function of temperature T. In the context of small rotations, the expression of the torsional wire stiffness provided by the SMA wire is:

$$K_{\theta_{SMA}} = F(T)\frac{R_t L}{L - R_t} \tag{12}$$

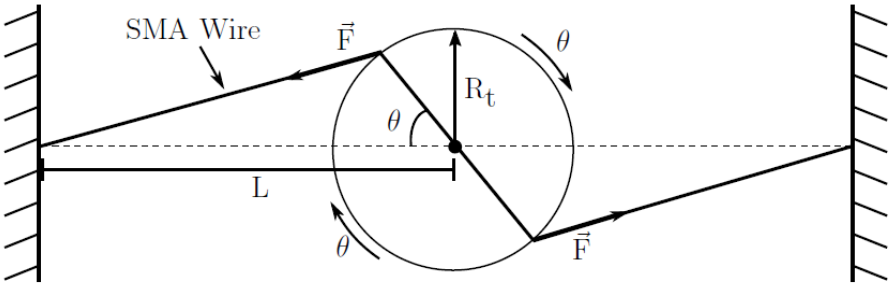

Figure 8. SMA assembly in the aeroelastic apparatus.

Initially, three different SMA wires (ARC-01,VIM-40,EB-03) with different proprierties were available to use. In order to verify which SMA provides the largest axial load, an experimental setup was proposed to measure the axial load of the wire in response to its temperature change. The wires were deformed up to 8% strain and kept at this deformation in order to prevent shape recovery during heating by Joule effect using a controlled current source, where the axial load for each SMA wire as a function of temperature is shown in Figure 9.

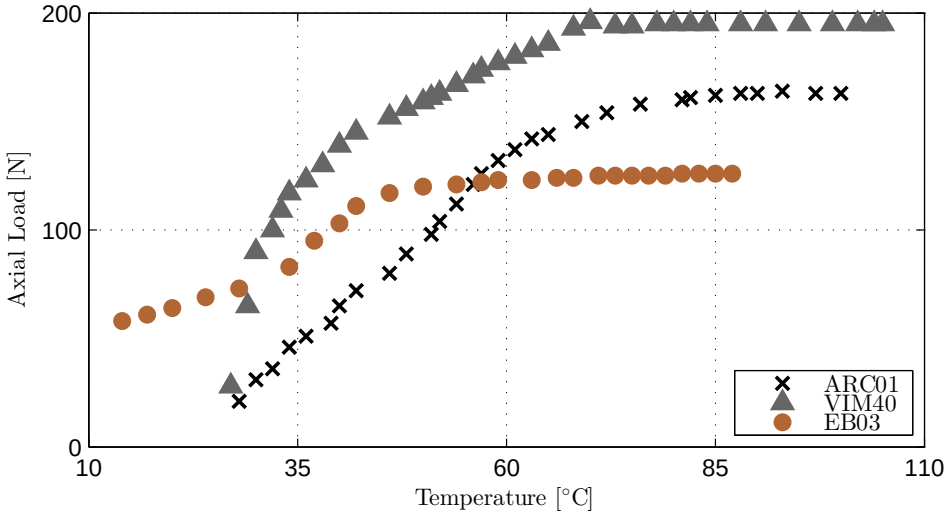

Figure 9. Axial load measured for the SMA wires phase transformation during the heating process.

Based on the satisfactory axial load response while in austenite phase, the 'VIM-40' wire was chosen to be applied in the wind tunnel tests to verify the applicability of the wire for oscillation reduction of the wing section. The VIM-40's chemical composition used in experiments is 49.42% of Ni, with 1.2 mm in diameter, and martensitic phase transformation temperatures of $A_s = 65.3°C$, $A_f = 91.0°C$, $M_s = 62.5°C$, and $M_f = 38.0°C$. Where, M_s is the start of temperature transformation of direct martensitic, M_f is the final temperature of direct martensitic transformation, A_s is the temperature at the beginning of the reversion of martensite to austenite, and A_f is the final temperature of the reversion of martensite to austenite.

Figure 10 shows the simulated accelerations at the typical section's leading edge with flow velocity of 14.5 m/s with the passive control applied at t $= 25$ s - the simulation starts in open loop, then the NiTi wire starts to be heated by Joule's effect from $t = 25$ s on, reducing the oscillations. The temperature response is shown at the bottom of the Figure 10.

Wind tunnel tests were performed for velocities from 14 m/s up to 15.5 m/s. During the tests the initial temperature of the wire was $23°C$, and after heating, final temperatures were $78°C$ for flow velocity of 14 m/s and $73°C$ for flow velocity of 14.6 m/s. Leading edge accelerations for flow velocities of 14 and 14.6 m/s can be seen in Figures 11 and 12, respectively.

As can be seen in Figures 11 and 12, with the increase in temperature, the composition of the SMA starts to change, increasing the Young modulus of the material. As a result, the torsional stiffness increases and the oscillations drop significantly. For a flow velocity of 14 m/s , the average acceleration in the first 10 s is 3.18 m/s^2 and drops to 0.65 m/s^2 in the last 10 s, which is 20.47% of the initial average. The reduction in the average acceleration at the leading edge is even more pronounced for a flow velocity of 14.6 m/s: from 4.08 m/s^2 in the first 10s to 0.267 m/s^2 in the last 10 s, which represents only 6.51% of the non controlled case. The average vibration reduction of the passive system tests was -16.2914 dB.

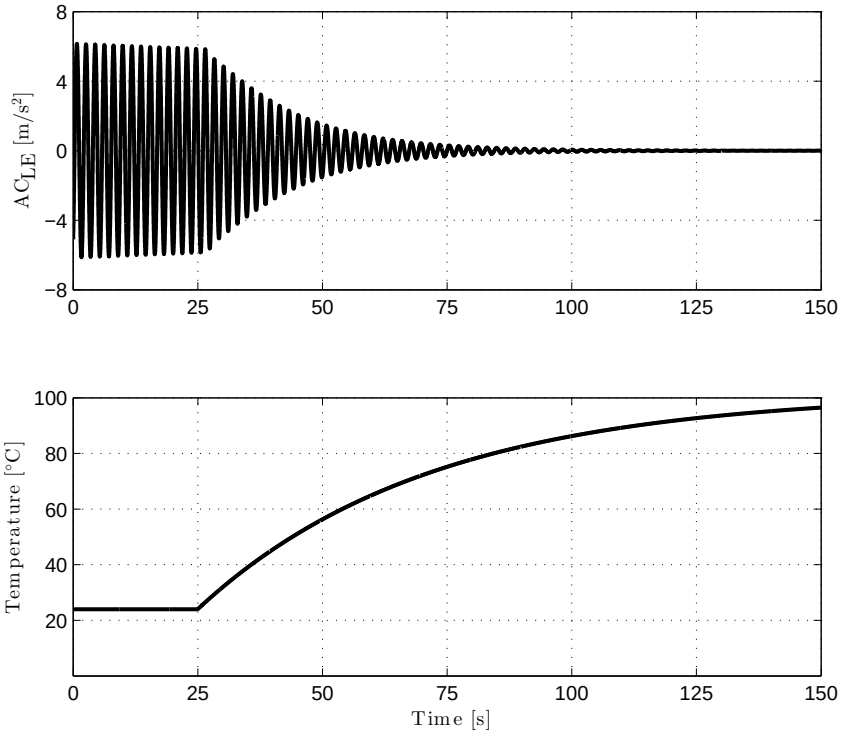

Figure 10. Simulated acceleration at the leading edge with velocity of 14.5 m/s (top) and the temperature response (bottom).

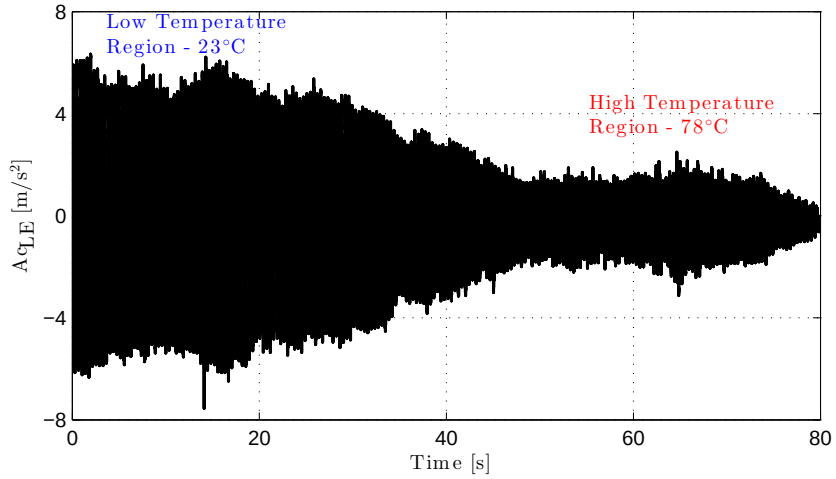

Figure 11. Leading edge measured acceleration at 14 m/s.

5. CONCLUSION

The passive control using SMA had a similar performance compared to the active control system and it is promising. Differently from the SAS that controls a flap directly, the application using SMA is less intrusive and does not change the flow characteristics, thus not resulting in an associated increase of drag.

6. ACKNOWLEDGEMENTS

The authors would also like to express special thanks to Prof. Dr. Jorge Otubo for manufacturing the Shape Memory Alloy wires and Prof. Luiz C. Sandoval Goes for providing the aeroelastic testbed and data acquisition systems.

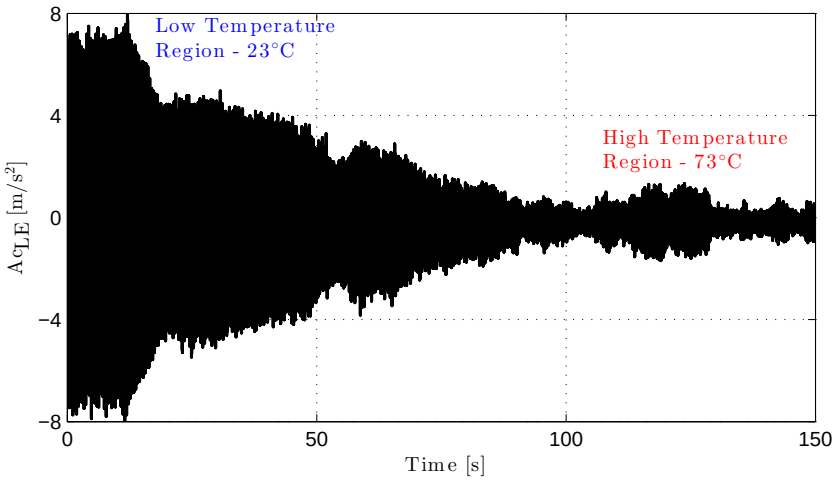

Figure 12. Leading edge measured acceleration at 14.6 m/s.

7. REFERENCES

De Marqui Jr, C., Belo, E.M. and Marques, F., 2004. "Wind-tunnel model and a controller for flutter suppression". In *45th AIAA/ASME/ASCE/AHS/ASC Structures, Structural Dynamics & Materials Conference*. pp. 19–22.

Donadon, M.V. and de Faria, A.R., 2016. "Aeroelastic behavior of composite laminated shells with embedded sma wires under supersonic flow". *Aerospace Science and Technology*, Vol. 52, pp. 157–166.

Dykman, J., Truong, H. and Urnes, J., 2013. "Active control for elastic wing structure dynamic modes".

Hwang, C. and Pi, W., 1984. "Optimal control applied to aircraft flutter suppression". *Journal of Guidance, Control, and Dynamics*, Vol. 7, No. 3, pp. 347–354.

Janocha, H. *et al.*, 1999. *Adaptronics and Smart Structures*. Springer.

Silva, G.C., Silvestre, F.J., Donadon, M.V. and Santos, O.S., 2017. "Active and passive control for acceleration reduction of an aeroelastic typical wing section". *Journal of Vibration and Control*.

Silvestre, F.J. and Luckner, R., 2015. "Experimental validation of a flight simulation model for slightly flexible aircraft". *AIAA Journal*, Vol. 53, No. 12, pp. 3620–3636.

Vipperman, J.S., Clark, R.L., Conner, M. and Dowell, E.H., 1998. "Experimental active control of a typical section using a trailing edge flap". *Journal of Aircraft*, Vol. 35, No. 2, pp. 224–229.

Wright, J.R. and Cooper, J.E., 2008. *Introduction to aircraft aeroelasticity and loads*, Vol. 20. John Wiley & Sons.

8. RESPONSIBILITY NOTICE

The authors are the only responsible for the printed material included in this paper.